Porous carbonized graphene-embedded fungus film as an interlayer for superior Li-S batteries

Liyuan Chai[a,b,1], Jiexi Wang[a,c,1], Haiying Wang[a,b,1], Liyuan Zhang[a,e,*], Wanting Yu[d], Liqiang Mai[c,*]

[a]School of Metallurgy and Environment, Central South University, Changsha 410083, PR China
[b]Chinese National Engineering Research Center for Control & Treatment of Heavy Metal Pollution, Central South University, Changsha 410083, PR China
[c]State Key Laboratory of Advanced Technology for Materials Synthesis and Processing, Wuhan University of Technology, Wuhan 430070, PR China
[d]Department of Environmental Monitoring, Changsha Environmental Protection College, Changsha 410004, PR China
[e]Environmental Engineering Research Centre, Department of Civil Engineering, the University of Hong Kong, Hong Kong, PR China

Abstract
Graphene-embedded carbon fiber (GFC) film has been fabricated by using filamentous fungus (*Aspergillus niger*) as carbonizable fibers to drive the graphene nanosheets to embed in the hyphae network system and then carbonizing at 700 °C. The molecular structure of the GFC film is primarily composed of aromatic components, and the film is doped by N (8.62%) and O (8.12%) elements. The conductivity of the final product reaches as high as $0.71\,S\,cm^{-1}$. The GFC film serves as the conductive interlayer to greatly improve the performance of Li-S batteries including capacity retention and rate capability. By inserting the GFC film, the battery can deliver a capacity of $\sim 700\,mAh\,g^{-1}$ after 300 cycles at 1 C. Even performed at 5 C, it is able to deliver a reversible capacity of more than $650\,mAh\,g^{-1}$. This research presents a facile and effective method for the fabrication of superior macroscopic carbon monolith, which holds great potential in other forms of electrochemical energy storage.
© 2015 Elsevier Ltd. All rights reserved.

*Corresponding author.
E-mail addresses: zhang_livyl@csu.edu.cn, lyzhk@hku.hk (L. Zhang), mlq518@whut.edu.cn (L. Mai).
[1]Liyuan Chai, Jiexi Wang and Haiying Wang contributed equally to this work.

Introduction

The development of sustainable electric systems (e.g., vehicles) has been an inconvertible trend all over the world, which significantly requires advanced rechargeable batteries with high energy density and good cyclability [1-4]. Lithium-sulfur (Li-S) batteries as a promising alternative possess high theoretical capacity (1675 mA h g^{-1}) and energy density (2600 Wh Kg^{-1}) [5]. Because of many advantages of sulfur (e.g., abundant resource, low cost, harmless), Li-S batteries have been recognized as one of the most competitive choices for the next generation electrochemical energy storage [6]. Unfortunately, the current Li-S batteries cannot totally fulfill the expectations of researchers, which limits its commercialization. One main reason is the insulating nature of sulfur and its lithiumization compounds (or named polysulfides), which lowers the cycling performance and rate capability [7]. Another one is that the polysulfide is readily dissolved in liquid electrolyte, which can transport through the separator to the anode. This phenomenon is called "shuttle effect" and inevitably decreases the coulombic efficiency and cyclability of the batteries [7].

To circumvent the aforementioned challenges, lots of methods have been proposed, which mainly concentrates on cathodes improvement. Successful examples include infiltrating the sulfur into various carbonaceous materials (e.g., reduced graphene oxide, carbon nanotubes, porous carbon) [4,8-18], using metal-organic framework as host to storage the sulfur [19,20], and covering traditional cathodes with polymers [21,22]. These methods not only restrict the shuttle effect, but also withstand the sulfur volume change. Apart from the above methods, it is also reported that coating or covalently bonding the sulfur with conducting polymers is very effective to suppress the dissolution and transportation of polysulfides, resulting in enhanced cyclability [23,24]. The modifications of sulfur cathodes indeed make the future of Li-S batteries more promising, but their fabrications are relatively complex and expensive [5], which restricts the large-scale applications of Li-S batteries.

Most recently, modifying cell configuration through inserting a conductive interlayer shows unexpected potential on improving the cyclability and capacity of Li-S battery. The conductive interlayer blocks the migration of the dissolved lithium polysulfides and readily reduced the potential polarization [25]. Until now, carbon black, multi-walled carbon nanotubes, conducting polymers, reduced graphene oxide and metal have been used to construct the conductive interlayer [25-32]. However, the procedures of preparing the interlayer by these raw materials are still relatively time consuming and complex. To further enhance the potential of interlayer, biomass-derived carbonaceous materials have been designed and synthesized. Leaf, cassava and eggshell were used as feedstock to obtain the porous biomass-derived carbon [33-36]. For the sake of practical applications, the carbonaceous materials need be assembled into a film by binders and this complicated the process. In an alternative way, paper towel and filter paper were carbonized to biomass-derived film acting as conductive interlayer, which avoided the introduction of binders [37,38]. But the performance of the battery is still needed to be improved as compared with that using graphene or carbon nanotubes as interlayer.

In present research, we design a microorganism-based approach for fabricating conductive porous carbon film (GFC film) through using filamentous fungus as carbonizable binders to stabilize the graphene nanosheets within the film. The film precursor is formed by a simple vacuum filtration of the mixture of graphene nanosheets and fungus hyphae suspension, which costs less than 1 min and is able to be easily scaled up. Moreover, the usage of filamentous fungus to prepare the carbon film satisfies the green and sustainable purpose. Furthermore, the nature of fungus decides high-content N element in the final product. This is beneficial to improve the performance of Li-S cells because the binding of sulfur-containing species at the N sites is more stable than binding on a carbon site [4]. The obtained film is expected to improve the performance of Li-S batteries when used as interlayer.

Experimental section

Materials

Graphene nanosheets powders were donated by The Sixth Element (Changzhou) Ltd. *Aspergillus niger* was provided by China Center for Type Culture Collection (CCTCC). Without special caution, the chemicals used were of analytical grade.

Culture of fungus

Potato medium was adopted to culture the fungus. Specifically, 200 g of potato was sliced and cooked in boiling water for 30 min. The potato was collected by gravity filtration using a gauze and the filtrate was put into a conical flask. Then 20 g of glucose, 0.05 g of MgSO$_4$·7H$_2$O and 0.1 g of KH$_2$PO$_4$ were added into the potato juice. The mixture solution (or potato medium) was treated at 115 °C under high pressure for 30 min. The fungus hyphae was inoculated into the potato medium. The culture temperature is 33 °C and the time is ~2 days.

Preparation of fungus hyphae dispersion

Fungus mycelium pellets were gradually formed during the solution culture of *Aspergillus niger*. The pellets were treated by a juice machine for 6 min, which became the dispersed hyphae. The hyphae were rinsed with deionized water for 5 times and collected by vacuum filtration. The hyphae were dispersed in mixture of water and ethanol (volume ratio 1:1) again to generate a suspension with a mass concentration of 10 mg mL^{-1}.

Synthesis of GFC film

1 g graphene nanosheets were dispersed in 50 mL 0.01 wt% of Tween aqueous solution for 150 min by ultrasonication (100 W). The graphene nanosheets dispersion was then poured into 400 mL of fungus hyphae suspension. The mixture was stirred vigorously for 10 min by electric blender with speed 1500 rounds per minute. To prepare the GFC film, 10 mL of black mixture was treated by vacuum
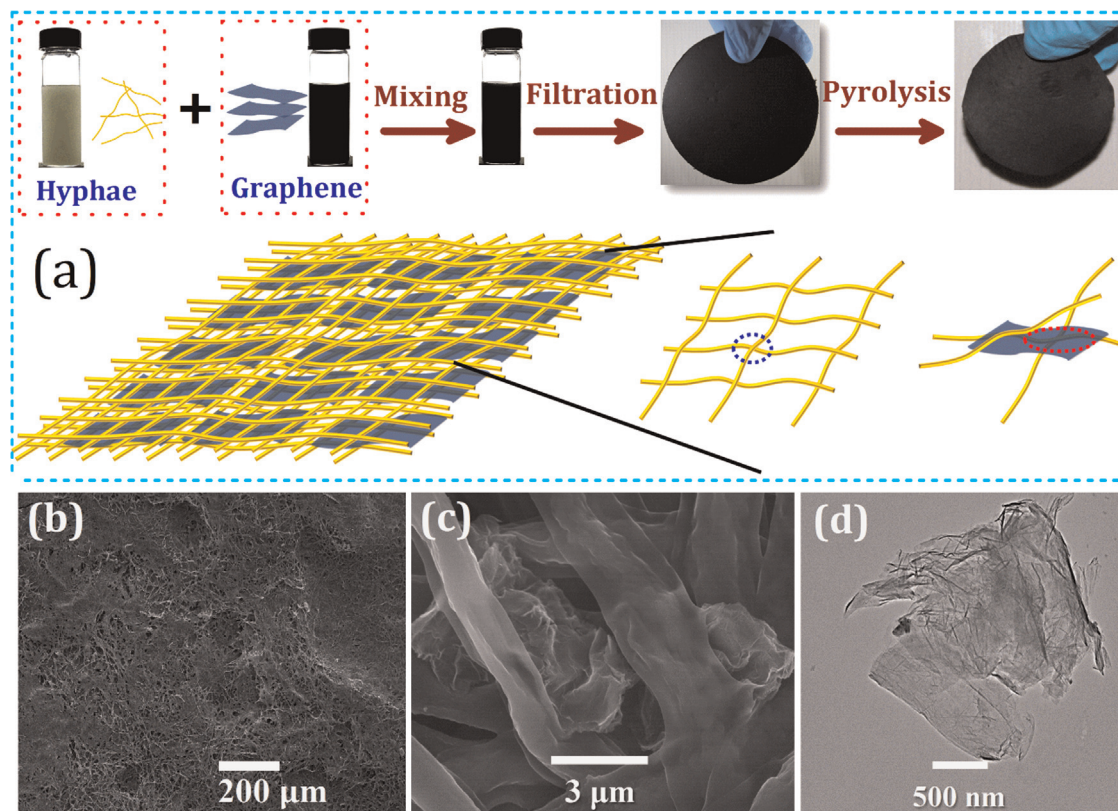
Fig. 1 (a) Flow diagram of the synthesis of GFC film and illustration of the configuration of the hybrid film, hyphae–hyphae interaction and graphene–hyphae interaction; SEM images of the GFC film with two different magnifications: (b) × 500, (c) × 20000; (d) TEM image of graphene nanosheets.

filtration with G-2 sand-core funnel, during which a free-standing black film was acquired. The film was dried for 12 h at 60 °C under flowing air. The dried film was annealed at 700 °C for 1 h in an inert atmosphere by tube furnace. After carbonization, the tube was cooled to room temperature naturally.

Characterization

Fourier transform infrared spectroscopy (FTIR), X-ray photoelectron spectroscopy (XPS) and Raman spectroscopy were applied to analyze the structural variation of the fungus. The sample was examined by Nicolet IS10 IR spectroscopy in the range of 4000–1000 cm^{-1} with resolution of 4 cm^{-1}. LABRAM-HR 800 Raman spectrometer was employed in the range of 3000–1000 cm^{-1} with a He–Le laser excitation at 513 nm and an acquisition time of 10 s. XPS measurements were made on ESCALAB 250Xi spectrometer with dual anode (Mg/Al) X-ray source with 400 W power. To compensate for surface charging effects, all binding energies were referenced to the C1s neutral carbon peak at 284.6 eV. Scanning electron microscope (SEM, JSM-6360) was adopted to investigate the morphology of the samples. The accelerating voltage is 20 kV. Energy dispersive spectrum was obtained by energy dispersive X-ray spectrometric microanalyzer (EDS, EDX-GENESIS 60S). The electron conductivity of the sample was examined by four probe method (RTS-9 4-point probes resistivity measurement systems). Micromeritics ASAP2010 Accelerated Surface Area and Porosimetry System

was used to analyze the sample. Before the measurement, the sample was degassed at 150 °C for 24 h. During the detection, the temperature was cooled by liquid nitrogen and the relative pressure was controlled from 0.01 to 1.

Cell assembly

To prepare the cathode, sulfur, carbon black and polyvinylidene fluoride with weight ratio of 6:3:1 were mixed with N-Methyl-2-pyrrolidinone to form a homogeneous slurry. Then, the slurry was coated on an aluminum current collector (20 μm, thickness) using a doctor-blade and dried in vacuum at 60 °C for 24 h. The 2025 coin-type cells with and without GFC interlayer between sulfur-containing cathode and separator (Celgard 2400) were assembled in the argon-filled glove box. The electrolyte was 1 M LiCF$_3$SO$_3$ (LTFSI, 99.95%, Aldrich) and 0.1 M LiNO$_3$ in the 1,3-dioxolane (DOL, 99.5%, Acros Organics) and 1,2-dimethoxyethane (DME, 99%, Acros Organics) mixed solvent (volume ratio of 1:1). The metallic lithium plate was used as anode.

Electrochemical performance

Cyclic voltammograms (CV) were measured with a CHI-660D electrochemical workstation at a scan rate of 0.1 mV s^{-1} in the voltage window of 3.0–1.5 V. Galvanostatic cycling was carried out with applying a LANDCT2001A battery cycler in the voltage range of 3.0–1.5 V (vs. Li$^+$/Li). For electrochemical impedance

spectroscopy tests, the frequency window was between 1 MHz and 0.01 Hz with an amplitude of 5 mV.

Results and discussion

Fig. 1a illustrates the two-step routes to fabricate the GFC film. The first step is to create a flexible film as carbon precursor by vacuum filtrating the mixture of hyphae and graphene nanosheets. In this step, the filamentous fungus serves as binders to stabilize the graphene nanosheets in the film. The completed film is formed in only 1 min. Subsequently, the film is dried and pyrolyzed at 700 °C to generate a black carbonaceous film. The graphene nanosheets in the film are mechanically stable and do not depart from the film. Fig. 1b provides the SEM images of GFC film. It is found that the film is porous. Fig. 1c reveals that the graphene nanosheets are embedded within the carbon fibers. Noticeably, the fungus is uniform belts in morphology (Fig. S1) while the graphene components are the plates (Fig. 1d). The gap size on the GFC film is less than 3 μm. As compared with the GFC film at present research, the fungus film prepared without graphene nanosheets possesses larger gap with size more than 10 μm (Fig. S2). The large gap in fungus film is obviously occupied by graphene nanosheets to form the GFC film. Noticeably, the fabrication of carbon precursor can be readily scaled up, which is dependent on the size of funnel. On the other hand, fungus used here is harmless to human beings and can be cultured at industrial scale, which is similar to other biomass [39,40]. This is the common advantage of microorganisms-based route to fabricate the carbonaceous materials [41]. These advantages are beneficial for the practical application of the final product.

To understand the formation of the film, the surface section structure of fungus was analyzed by FTIR (Fig. 2a). The peaks at 1041 and 1067 cm^{-1} are attributed to the stretching vibration of polysaccharides [42]. The three peaks in the range of 1700–1300 cm^{-1} are the typical IR adsorption signals of amide groups of proteins [42]. That is to say, the surface section of the fungus contains the proteins and polysaccharides [43]. In general, polysaccharides are the dominated components in the cell wall, which acts as robust backbone to shape the morphology of the funugs. Moreover, it is recently revealed that a flexible film can be formed through the vacuum filtration of the dispersed hyphae, which is mostly caused by the strong interaction of wet polysaccharides on the cell wall (Fig. 2b and Fig. S3) [42-44]. The sharp peaks between 3000-2700 cm^{-1} and another one at ~1230 cm^{-1} are related to the lipid, which may come from the cell membrane [42]. It is believed that small amounts of lipid on the cell wall can regulate the hydrophobicity of the fungus surface. It is possible that the vacuum filtration of the mixture of hyphae and graphene nanosheets force the ultimate hyphae-graphene contacts and the lipid interacts with the graphene through hydrophobic forces (Fig. 2c). Together, we believe that the hyphae-hyphae contact is the basis for the formation of the film. During the film formation, the hyphae-graphene interaction promises the adhesion of the graphene nanosheets onto the hyphae film, as demonstrated in Fig. 1a. It is also possible that the graphene nanosheet
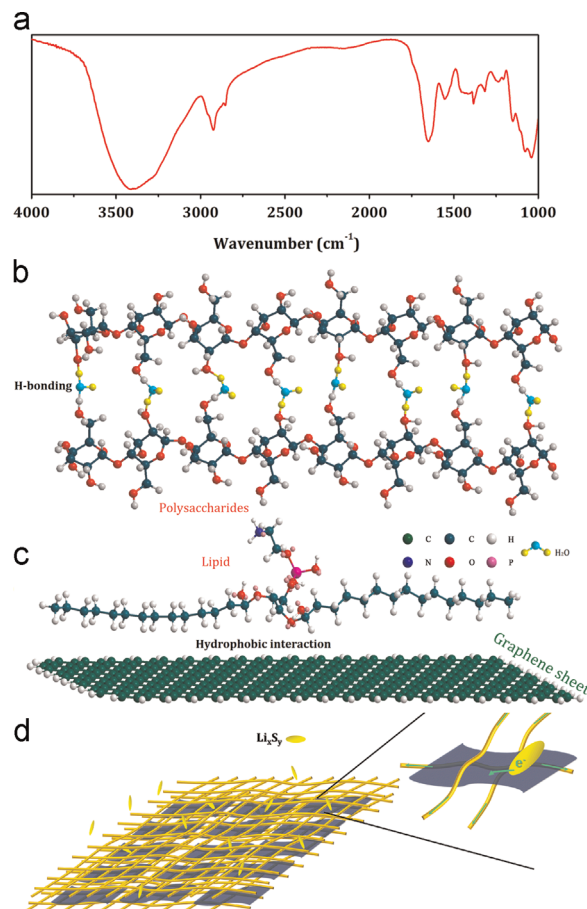

Fig. 2 (a) FTIR spectrum of the fungus (*Aspergillus niger*). Illustration of the possible formation routes of graphene-embedded fungus film; (b) hydrogen bonding between polysaccharides from the cell wall and (c) hydrophobic interaction between lipid and graphene nanosheets; (d) function of the GFC inserting Li-S batteries.

was squeezed between two hyphae. The deep mechanism on the hybrid film formation is still unclear and much effort is needed. The interlayer is expected to function as the shield to prevent the shuttling of Li$_x$S$_y$ (Fig. 2d), which will be revealed later.

The Raman technique was further applied to investigate the structural variation of the sample (Fig. 3a and Fig. S4). In terms of fungus, only a broad peak is detected, which is ascribed to the fluorescence effect. After the hybrid film composed of fungus and graphene nanosheets is treated at 700 °C to become GFC film, three peaks located at ~1340, ~1590 and ~2700 cm^{-1} are found, corresponding to the G band, D band and 2D band, respectively. That means the GFC film exhibits a relatively good graphitization degree. The graphitization degree of the fungus-derived carbon is relatively low (Fig. S5), which indirectly demonstrates the important contribution of graphene nanosheets on improving the graphitization of the final product. FTIR technique was also used to analyze the structural variation of the GFC film. As compared with the fungus, GFC film possess nearly no IR adsorption (Fig. S6). The functional groups of fungus disappear after treating at high temperature, which is a prerequisite for the formation of partially graphitized carbon.
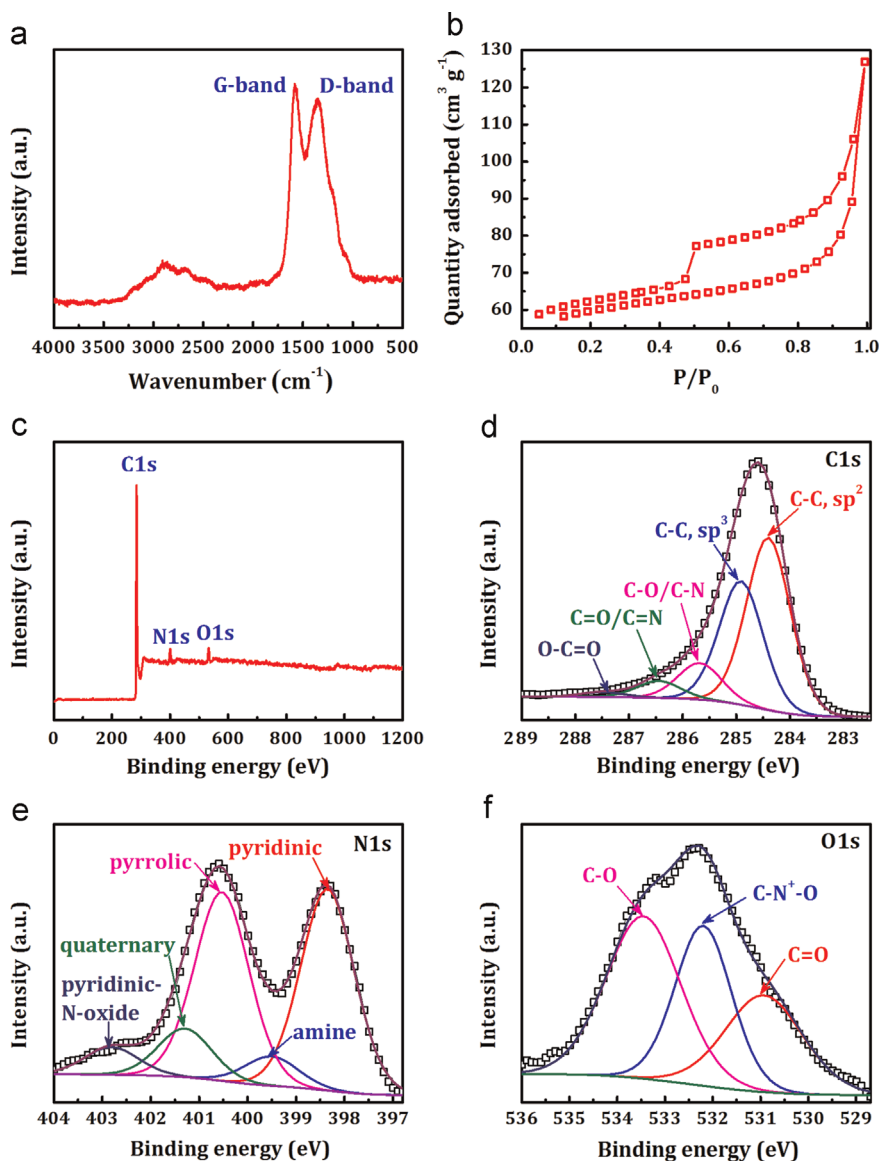
Fig. 3 (a) Raman spectrum of GFC film; (b) N_2 adsorption-desorption isotherm of GFC film; (c) XPS spectrum of GFC film; (d) C1s spectrum; (e) N1s spectrum and (f) O1s spectrum.

As a consequence, a good conductivity of $0.71\,S\,cm^{-1}$ was measured based on four-probe method. This conductivity is superior as compared to other biomass-derived carbons, which were generally prepared aftre heat treatment at $>800\,°C$ (Fig. S7) [43,45,46]. Based on the nitrogen adsorption-desorption test, the film possesses surface area more than $200\,m^2\,g^{-1}$ and abundant mesopores with narrow pore size around 40 nm and pore volume about $0.12\,cm^3\,g^{-1}$ (Fig. 3b and Fig. S8).

The GFC film was further characterized with XPS technique, as dispalyed in Fig. 3c-f and Table 1. Based on the C1s spectrum and calculation, the GFC film is mainly composed of sp^2 carbon (48.66%). Other chemical bonds are sp^3 carbon (34.87%), C-O/C-N (10.31%), C=O/C=N (4.76%) and O-C=O (1.4%). The analysis of C1s spectrum demonstrates that the carbon film is doped by abundant heteroatoms such as O and N. According to the peak area in Fig. 3c, the N and O elements account for 8.62% and 8.12% of the total element, respectively. The deconvolution of N1s and O1s spectra

further verifies the heteroatom doping nature of the GFC film. Typically, pyridinic and pyrrolic conjugated structures dominate in total components. The heteroatoms doping can improve the properties of carbonaceous materials, including conductivity, wettability and so forth [47-49], and thus the N/O doping potentially affords superior application performance for GFC film.

Inspired by the porous structure, good electrical conductivity, and potential superior filling and adsorptive properties, the GFC film was applied as conductive interlayer to provide gradients for suppressing the diffusion of polysulfides, and thus to improve the electrochemical performance of Li-S batteries. Fig. 4a compares the cyclic voltammetry (CV) curves of the batteries with and without the GFC interlayer. The active material loadings for both cells are almost the same (about $1.2\,mg\text{-}S\,cm^{-2}$). The cathodic peak at about 2.25 V indicates the transformation of sulfur to long-chain polysulfides and the following cathodic peak at

| Element	Chemical bonds	Binding energy (ev)	Atomic ratio (%)
C	sp^2	284.4	48.66
	sp^3	284.9	34.87
	C–O/C–N	285.7	10.31
	C=O/C=N	286.4	4.76
	O–C=O	287.5	1.40
N	Pyridinic	398.4	41.40
	Amine	399.5	3.58
	Pyrrolic	400.5	39.34
	Quaternary	401.3	10.00
	Pyridinic-N-oxide	402.8	5.68
O	C=O	530.9	10.97
	C–N$^+$–O	532.2	37.96
	C–O	533.4	51.07

about 2.07 V can be signified as the subsequent reduction of the long-chain polysulfides to Li_2S_2/Li_2S. The two overlapping peaks between 2.32 and 2.58 V during the anodic stage are ascribed to the gradual oxidation of Li_2S_2/Li_2S to Li_2S_8/S_8. It can be clearly seen that the cell with GFC interlayer shows higher current peaks than the cell without interlayer, indicating stronger electrochemical kinetics and better utilization of active mass of the GFC-interlayer-modified cell. The initial charge-discharge curves at 0.5 C rate (1 C=1675 mA g^{-1}-S) in Fig. 4b demonstrate that the cell without GFC shows lower discharge plateaus while higher charge plateaus than the cell with GFC, revealing that the insertion of GFC is able to enhance the electrochemical reaction and lower the electrode polarization. This is in accordance with the CV results that the anodic peak of the cell with GFC shifts to lower potential (with potential difference $\Delta U=0.08$ V) compared to that of the cell without GFC. It is noted that the initial Coulombic efficiencies are relatively high, which is due to the addition of $LiNO_3$ that has positive effect on hindering the reaction between polysulfides and Li anode [50,51]. However, the cell with GFC possesses nearly 100% Coulombic efficiency, which is higher than the cell without GFC. This phenomenon is attributed to that the GFC interlayer acts as a secondary active materials collector, trapping polysulfides and thus improving the electrode reversibility. From Fig. 4b, we also see that the cell with GFC interlayer delivers much higher reversible specific capacity ($\sim$1250 mAh g^{-1}-S) than that without GFC ($\sim$545 mAh g^{-1}-S). Fig. 4c compares the cycling performance of both cells at 1 C rate. Compared to rapid capacity fading of the cell without GFC from 493 to 318 mAh g^{-1}-S in 20 cycles, the cell with GFC interlayer exhibits greatly improved cycling performance, maintaining a reversible capacity of 698 mAh g^{-1}-S after 300 cycles. It is

noted that for the cell with GFC interlayer, except for obvious capacity fading during the first several cycles, the capacity keeps stable in subsequent cycling process. Particularly, in the first 5 cycles, the reversible capacity decreases from 1138 to 995 mAh g^{-1}-S. After that, only about 1 mAh g^{-1}-S fading per cycle is found. The phenomenon of fast capacity fading during the first several cycles may be due to formation and dissolution of lithium polysulfides before the concentration of dissolved polysulfides reached equilibrium. The rate capability of the batteries with or without the GFC film was investigated at the current densities in the range of 0.5-5 C. As given in Fig. 4d, the GFC-film-inserted battery delivers a capacity of more than 1000 mAh g^{-1} at 0.5 C. When gradually increasing the current rate from 0.5 to 5 C, the corresponding capacity drops orderly, but the delivered capacity at 5 C still remains the level of more than 650 mAh g^{-1}-S. As the current rate is returned to 0.5 C, a stable capacity of $\sim$960 mAh g^{-1}-S can be achieved. As compared with the GFC-film-inserted batteries, the original one displays only 400-500 mAh g^{-1}-S at 0.5 C. When the current rate is promoted to 5 C, the capacity further declines to less than 100 mAh g^{-1}. The performance of the Li-S batteries based on the conductive interlayer in current work is superior as compared with the previous reports on developing biomass-derived carbon interlayer (Fig. S9) [34-38,43]. This promises the application of GFC film in the future. Therefore, it can be concluded that the GFC interlayer is able to improve the electrochemical performance of Li-S batteries. One of the reasons may be that the GFC interlayer plays a conductive collector that would decrease the resistance against electron/ion transfer, and promote the electrochemical reaction by providing large and steady reaction space. To verify such hypothesis, EIS tests after 50 cycles were conducted. As shown in Fig. 4e, the Nyquist plots of both samples are composed of one intercept at very high frequency indexed with ohmic resistance of the cell (R_e), two semicircles from high to middle frequency which separately correspond to interface contact impedance (high frequency, $R_{sf}//CPE_{sf}$) and charge transfer impedance (middle frequency, $R_{ct}//CPE_{dl}$), and a slope line corresponds to Warburg impedance. The EIS data were fitted with the equivalent electrical circuit as shown in the inset of Fig. 4e. The cell with GFC film shows less value of R_{sf} (2 Ω) than the cell without interlayer (8 Ω), indicating enhanced wettability and better lithium ion diffusion at the electrode/electrolyte interface in the GFC-film-modified cells. Due to the GFC interlayer also provides large reaction area, the charge transfer during the interfacial electrochemical reaction are promoted. As a result, the R_{ct} value of the cell with GFC film (4 Ω) is much smaller than that of the bare cell. Moreover, it is a fact that the dissolution of polysulfides results in deterioration of conductivity of the electrolyte. Therefore, the phenomenon of the GFC film modified cell possessing smaller R_e values than the pristine cell confirms that the GFC interlayer has ability to trap polysulfides and then suppress the shuttle effect.

To verify this concept, the GFC film after 50 cycles was characterized by SEM and EDS techniques. As shown in Fig. 5a–c, the holes of the film observed in Fig. 3b is filled, and a uniform and smooth substance is coated onto the GFC
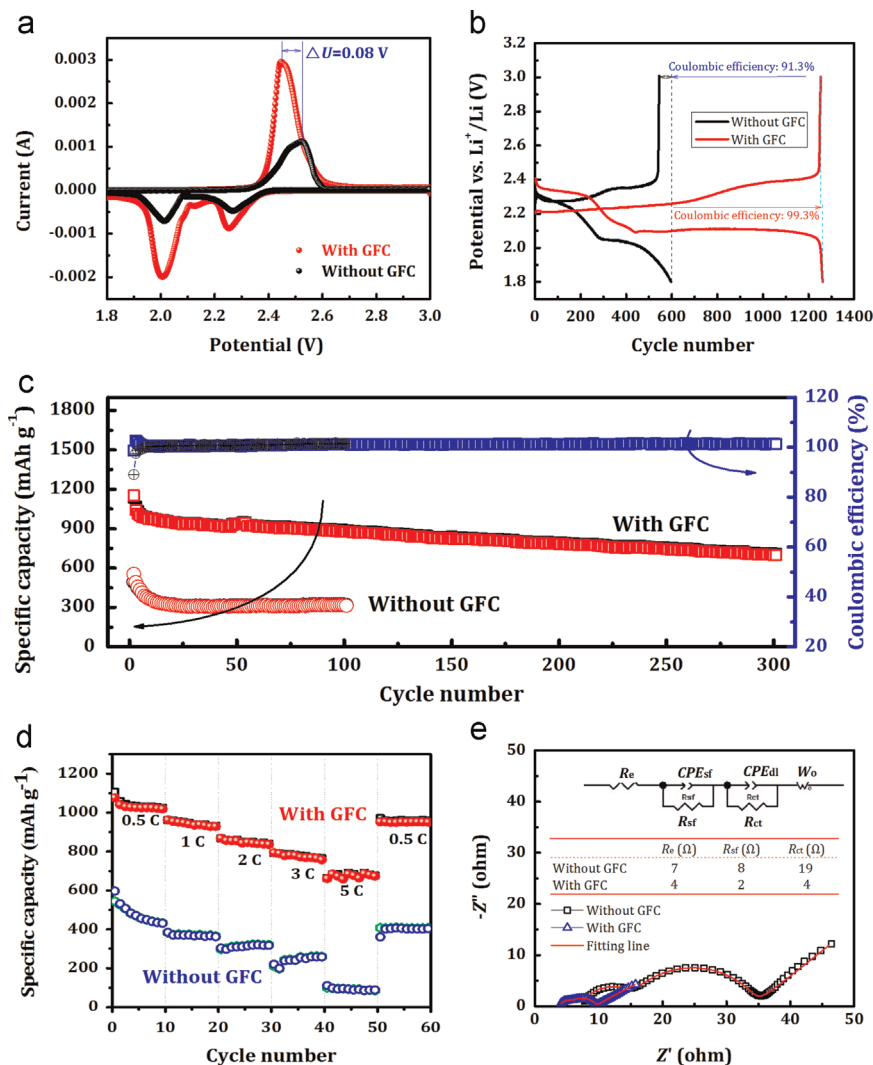
Fig. 4 (a) CV curves of the Li-S batteries with (red line) and without (black line) GFC interlayer; (b) initial discharge-charge curves of Li-S cells with (red line) and without (black line) GFC interlayer at 0.5 C rate; (c) cycling performance of Li-S cell without GFC and with interlayer at 1 C rate; (d) rate capability of the Li-S cells with and without GFC interlayer in the current range of 0.5-5 C rate; (e) EIS plots of the Li-S cells with (blue dots) and without (black dots) after 50 cycles. Each electrode weighs about 1.2 mg-S cm^{-2}.
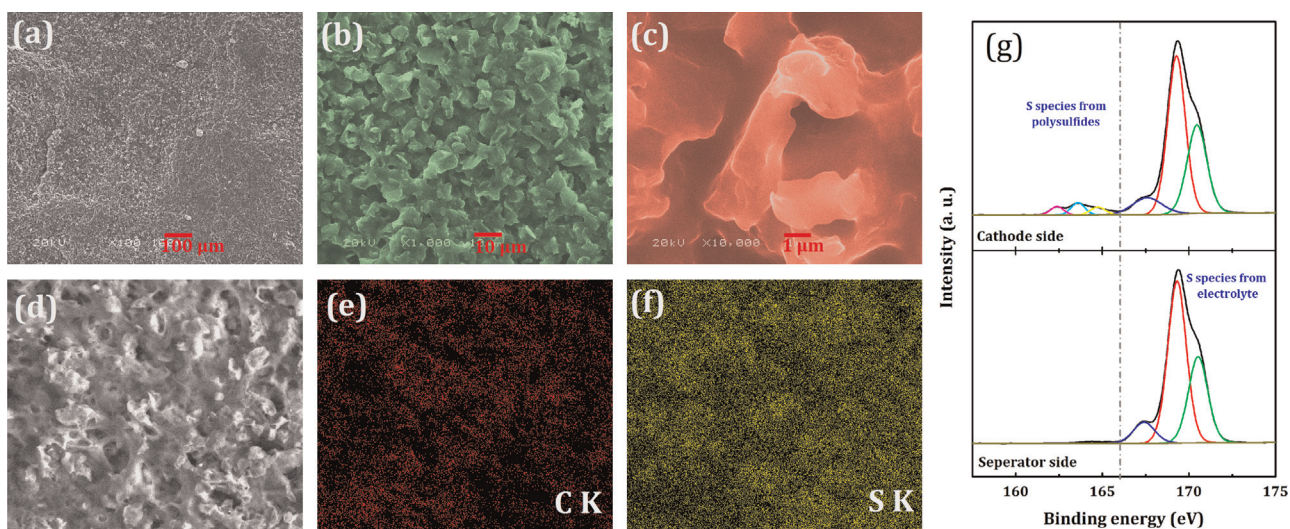
Fig. 5 (a–c) SEM images of the GFC film after 50 cycles; (d–f) EDS mapping images of the GFC film after 50 cycles; (g) XPS spectra of interlayer (two faces: cathode side and separator side) after 300 cycles at 1 C.

film. Fig. 5f further confirmed that abundant sulfur element exists. Furthermore, double sides of interlayer after 300 cycles at 1 C were analyzed by XPS. As seen in Fig. 5g, on the cathode side, S-S (163.6 eV) and Li-S (162.3 eV) bonding species are observed, indicating formation of polysulfide on the cathode side. While the content of these species on separator side is really low, which confirmed the shuttle blocking by intelayer. Moreover, sulfur distribution is also observed (Fig. S10) along the cross section. All of these no doubt prove the ability of the GFC film to restrict the shuttling of the polysulfides.

Conclusion

Filamentous fungus was adopted as the carbonizable binders to fabricate the graphene-embedded carbon fiber film, which is green, sustainable and large scale. The film is doped by N and O elements and exhibits high conductivity. The film serves as superior conductive interlayer for improving the performance of Li-S batteries. After 300 cycles at 1 C, the capacity of the batteries can still reach $\sim$700 mAh g^{-1}. Moreover, even at 5 C, the batteries can still exhibit a discharge capacity of $\sim$650 mAh g^{-1}. The improved Li-S batteries outperform the capability of many other reported examples. This research opens a hopeful window for the fabrication of superior macroscopic carbon monolith, which holds great potential in other forms of electrochemical energy storage.

Acknowledgments

Appendix A.   Supplementary material

Supplementary data associated with this article can be found in the online version at http://dx.doi.org/10.1016/j.nanoen.2015.09.001.

References

[1] L. Mai, X. Tian, X. Xu, L. Chang, L. Xu, Chem. Rev. 114 (2014) 11828-11862.
[2] X. Xia, D. Chao, Z. Fan, C. Guan, X. Cao, H. Zhang, H.J. Fan, Nano Lett. 14 (2014) 1651-1658.
[3] R.N. Nasim Khan, N. Mahmood, C. Lv, G. Sima, J. Zhang, J. Hao, Y. Hou, Y. Wei, RSC Adv. 4 (2014) 7374.
[4] K. Han, J. Shen, S. Han, H. Ye, C. Wolverton, M.C. Kung, H.H. Kung, ChemSusChem 7 (2014) 2545-2553.
[5] G. Zhou, S. Pei, L. Li, D.W. Wang, S. Wang, K. Huang, L.C. Yin, F. Li, H.M. Cheng, Adv. Mater. 26 (2014) 625-631 664.
[6] R. Chen, T. Zhao, F. Wu, Chem. Commun. 51 (2015) 18-33.
[7] A. Manthiram, Y. Fu, S.H. Chung, C. Zu, Y.S. Su, Chem. Rev. 114 (2014) 11751-11787.
[8] Z. Yuan, H.-J. Peng, J.-Q. Huang, X.-Y. Liu, D.-W. Wang, X.-B. Cheng, Q. Zhang, Adv. Funct. Mater. 24 (2014) 6105-6112.
[9] S. Zheng, F. Yi, Z. Li, Y. Zhu, Y. Xu, C. Luo, J. Yang, C. Wang, Adv. Funct. Mater. 24 (2014) 4156-4163.
[10] G. He, B. Mandlmeier, J. Schuster, L.F. Nazar, T. Bein, Chem. Mater. 26 (2014) 3879-3886.
[11] D.S. Jung, T.H. Hwang, J.H. Lee, H.Y. Koo, R.A. Shakoor, R. Kahraman, Y.N. Jo, M.S. Park, J.W. Choi, Nano Lett. 14 (2014) 4418-4425.
[12] L. Sun, M. Li, Y. Jiang, W. Kong, K. Jiang, J. Wang, S. Fan, Nano Lett. 14 (2014) 4044-4049.
[13] S. Evers, L.F. Nazar, Chem. Commun. 48 (2012) 1233-1235.
[14] X. Ji, K.T. Lee, L.F. Nazar, Nat. Mater. 8 (2009) 500-506.
[15] G. Zhou, Y. Zhao, C. Zu, A. Manthiram, Nano Energy 12 (2015) 240-249.
[16] D. Wang, Y. Yu, W. Zhou, H. Chen, F.J. DiSalvo, D.A. Muller, H.D. Abruna, Phys. Chem. Chem. Phys. 15 (2013) 9051-9057.
[17] C. Wu, L. Fu, J. Maier, Y. Yu, J. Mater. Chem. A 3 (2015) 9438-9445.
[18] L. Zeng, F. Pan, W. Li, Y. Jiang, X. Zhong, Y. Yu, Nanoscale 6 (2014) 9579-9587.
[19] J. Zhou, R. Li, X. Fan, Y. Chen, R. Han, W. Li, J. Zheng, B. Wang, X. Li, Energy Environ. Sci. 7 (2014) 2715.
[20] J. Zheng, J. Tian, D. Wu, M. Gu, W. Xu, C. Wang, F. Gao, M.H. Engelhard, J.G. Zhang, J. Liu, J. Xiao, Nano Lett. 14 (2014) 2345-2352.
[21] S.J. Oh, J.K. Lee, W.Y. Yoon, ChemSusChem 7 (2014) 2562-2566.
[22] Y. Yang, G. Yu, J.J. Cha, H. Wu, M. Vosgueritchian, Y. Yao, Z. Bao, Y. Cui, ACS Nano 5 (2011) 9187-9193.
[23] L. Xiao, Y. Cao, J. Xiao, B. Schwenzer, M.H. Engelhard, L.V. Saraf, Z. Nie, G.J. Exarhos, J. Liu, Adv. Mater. 24 (2012) 1176-1181.
[24] W. Zhou, Y. Yu, H. Chen, F.J. DiSalvo, H.D. Abruna, J. Am. Chem. Soc. 135 (2013) 16736-16743.
[25] Y.S. Su, A. Manthiram, Nat. Commun. 3 (2012) 1166.
[26] T.G. Jeong, Y.H. Moon, H.H. Chun, H.S. Kim, B.W. Cho, Y.T. Kim, Chem. Commun. 49 (2013) 11107-11109.
[27] Y.S. Su, A. Manthiram, Chem. Commun. 48 (2012) 8817-8819.
[28] S.-H. Chung, A. Manthiram, J. Phys. Chem. Lett. 5 (2014) 1978-1983.
[29] X. Wang, Z. Wang, L. Chen, J. Power Sources 242 (2013) 65-69.
[30] K. Zhang, F. Qin, J. Fang, Q. Li, M. Jia, Y. Lai, Z. Zhang, J. Li, J. Solid State Electrochem. 18 (2013) 1025-1029.
[31] C. Zu, Y.S. Su, Y. Fu, A. Manthiram, Phys. Chem. Chem. Phys. 15 (2013) 2291-2297.
[32] G. Ma, Z. Wen, J. Jin, M. Wu, X. Wu, J. Zhang, J. Power Sources 267 (2014) 542-546.
[33] S.-H. Chung, A. Manthiram, ACS Sustain. Chem. Eng. 2 (2014) 2248-2252.
[34] S.H. Chung, A. Manthiram, ChemSusChem 7 (2014) 1655-1661.
[35] F. Qin, K. Zhang, J. Fang, Y. Lai, Q. Li, Z. Zhang, J. Li, New J. Chem. 38 (2014) 4549-4554.
[36] S.H. Chung, A. Manthiram, Adv. Mater. 26 (2014) 1360-1365.
[37] K. Zhang, Q. Li, L. Zhang, J. Fang, J. Li, F. Qin, Z. Zhang, Y. Lai, Mater. Lett. 121 (2014) 198-201.
[38] S.H. Chung, A. Manthiram, Chem. Commun. 50 (2014) 4184-4187.
[39] W. Luo, J. Schardt, C. Bommier, B. Wang, J. Razink, J. Simonsen, X. Ji, J. Mater. Chem. A 1 (2013) 10662.
[40] W. Luo, B. Wang, C.G. Heron, M.J. Allen, J. Morre, C.S. Maier, W.F. Stickle, X. Ji, Nano Lett. 14 (2014) 2225-2229.
[41] L. Xiong, J.-J. Chen, Y.-X. Huang, W.-W. Li, J.-F. Xie, H.-Q. Yu, Nano Energy 12 (2015) 33-42.
[42] A.R. Badireddy, S. Chellam, P.L. Gassman, M.H. Engelhard, A.S. Lea, K.M. Rosso, Water Res. 44 (2010) 4505-4516.

[43] L. Zhang, Y. Wang, B. Peng, W. Yu, H. Wang, T. Wang, B. Deng, L. Chai, K. Zhang, J. Wang, Green Chem. 16 (2014) 3926-3934.

[44] A.E. Nel, L. Madler, D. Velegol, T. Xia, E.M. Hoek, P. Somasundaran, F. Klaessig, V. Castranova, M. Thompson, Nat. mater. 8 (2009) 543-557.

[45] N. Brun, S.A. Wohlgemuth, P. Osiceanu, M.M. Titirici, Green Chem. 15 (2013) 2514-2524.

[46] H.-W. Liang, Q.-F. Guan, Z. Zhu, L.-T. Song, H.-B. Yao, X. Lei, S.-H. Yu, NPG Asia Mater. 4 (2012) e19.

[47] H. Fei, R. Ye, G. Ye, Y. Gong, Z. Peng, X. Fan, E.L.G. Samuel, P. M. Ajayan, J.M. Tour, ACS Nano 8 (2014) 10837-10843.

[48] K.P. Singh, M.Y. Song, J.-S. Yu, J. Mater. Chem. A 2 (2014) 18115-18124.

[49] N. Ranjbar Sahraie, J.P. Paraknowitsch, C. Gobel, A. Thomas, P. Strasser, J. Am. Chem. Soc. 136 (2014) 14486-14497.

[50] S. Xiong, K. Xie, Y. Diao, X. Hong, Electrochim. Acta 83 (2012) 78-86.

[51] X. Liang, Z. Wen, Y. Liu, M. Wu, J. Jin, H. Zhang, X. Wu, J. Power Sources 196 (2011) 9839-9843.

Liyuan Chai received his Ph.D degree in Metallurgical Engineering from Central South University in 1995. He is now the Dean and Professor of School of Metallurgy and Environment, and director of Chinese National Engineering Research Center for Control & Treatment of Heavy Metal Pollution at Central South University in China. His research interest broadly lies in the reduction & resourcelization of heavy metal pollutant and bio-derived materials. He has published more than 100 papers in international journals including *Environmental Science & Technology, Water Research, Journal of Hazardous Materials, Bioresource Technology, Journal of Materials Chemistry, Langmuir, etc*.

Jiexi Wang received his Bachelor's degree in Metallurgical Engineering from Central South University in 2010. In 2015, He received his Ph.D degree in physical chemistry of metallurgy at School of Metallurgy and Environment, Central South University supervised by Prof. Xinhai Li. His research focuses on the synthesis and application of nanomaterials and biomass-derived composites for clean energy storage, such as high-power/high-energy lithium batteries and supercapacitors.

Haiying Wang got his Ph.D degree of Applied Chemistry at Nanjing University of Science and Technology in 2007. In 2014, he carried out research as a visiting scholar at Georgia Institute of Technology. He is now an associate professor at the School of Metallurgy and Environment of Central South University in China. His interest is mainly about the design and synthesis of novel functional nanomaterials for environmental purification and energy application.

Liyuan Zhang received his Ph.D degree of Environment Science from Central South University in 2015. He is now a postdoctoral fellow in Environmental Engineering Research Centre at the University of Hong Kong. His main research interests involve biomimetic materials, conjugated polymers, carbon materials and their applications. His research works have been published in *Green Chemistry, Chemical Communications, Journal of Materials Chemistry, Langmuir, Journal of Power Sources, Dalton Transaction, etc*.

Wanting Yu graduated from Central South University, where she received her B.Sc. degree in 2005 and M.Sc. degree in 2008 in chemical technology under the guidance of Professor Hui Wang, then received her Ph.D. degree in 2013 in environmental engineering under the direction of Professor Liyuan Chai. Her research interest is the wastewater treatment materials and technology.

Liqiang Mai received his Ph.D. from Wuhan University of Technology in 2004. He carried out his postdoctoral research in the laboratory of Prof. Zhonglin Wang at Georgia Institute of Technology in 2006-2007 and worked as advanced research scholar in the laboratory of Prof. Charles M. Lieber at Harvard University in 2008-2011. He is Chair Professor of Materials Science and Engineering at Wuhan University of Technology. He has published more than 110 papers tagged by SCI in peer-reviewed journals such as Nature Nanotechnology, Nature Communications, Chemical Reviews, Proceedings of the National Academy of Sciences, Journal of the American Chemical Society, Nano Letters, Advanced Materials, and so forth. His interests include nanowire materials, micro/nanoenergy storage devices, and energy-based nano-bio interface.